Improved Integration Method of Wide-area RTK/PPP with IMU and Odometer

Improved Integration Method of Wide-area RTK/PPP with IMU and Odometer

Nobuaki Kubo, Daisuke Hatta, Kaito Kobayashi, Kyohei Aoki, Tokyo University of Marine Science and Technology

BIOGRAPHY (IES)

Nobuaki Kubo received his B.S., M.S. in Electrical Engineering from Hokkaido University and doctorate in Engineering from University of Tokyo in 2005. He resided at Stanford University in 2008 as a visiting scholar. He is now an associate professor at Tokyo University of Marine Science and Technology, Japan. Member of Japan Institute of Navigation.
Daisuke Hatta is a 1th year graduate student at Tokyo University of Maritime Science and Technology. His research interest is integrated positioning using IMU and GNSS.
Kaito Kobayashi is a 1th year graduate student at Tokyo University of Maritime Science and Technology. His research interest is anti-spoofing and RTK/PPP applications.
Kyohei Aoki is a 1th year graduate student at Tokyo University of Maritime Science and Technology. His research interest is the improvement of algorithm in CLAS/MADOCA-PPP.

ABSTRACT

The Quasi-Zenith Satellite System (QZSS), Japanese positioning satellite constellation has two types of precise point positioning (PPP) services: centimeter-level augmentation service (CLAS) for land and multi-GNSS advanced demonstration tool for orbit and clock analysis (MADOCA). Currently, both CLAS and PPP correction data are broadcasted through the QZSS. It is highly good time to evaluate CLAS and PPP service in Japan. CLAS service has advantage in convergence time compared with PPP service. In the case of short gap like as overpasses, the convergence time is within 1 minute. The motivation of this research is to investigate the integration of CLAS or PPP results and our previous integration method using low-cost IMU/Odometer sensors. In reality, several commercial receivers capable of using CLAS or PPP correction services are already released in Japan. We used outputs of these receivers for absolute positions and loosely-coupled integration using Kalman filter is used to integrate them. The test data were obtained on the sea and expressway in 2019. Firstly, the performance of PPP and CLAS on the sea using the commercial receiver was evaluated. For the reference of these positions, normal RTK was obtained in parallel in this test on the sea. In the test on the expressway, POLSV was used in parallel to produce the precise positions as a reference. Looking at the test results on the sea, the fix rate of CLAS was from 63 % to 94. The standard deviation in horizontal was within 10 cm. On the other hand, the result of PPP was slightly worse than the result of CLAS. We didn't evaluate the integrated navigation on the sea because it was impossible for us to obtain the speed information from the ship for now. Looking at the test results on the expressway, the fix rate of CLAS was also good over 70 %. The navigation performance of this integrated system was analyzed. The horizontal accuracy including some GNSS outages was stable and the standard deviation of all horizontal errors was 0.35 m. The 99 percentile value for the absolute horizontal errors was 1.34 m. 99.57 % of all solutions were less than 1.5 m. With regard to the test results of PPP and integrated system on the expressway, the results were introduced in Pacific ION 2019.

INTRODUCTION

The real-time kinematic Global Navigation Satellite System (RTK-GNSS) and Precise Point Positioning (PPP) methods have been widely used for achieving centimeter- or decimeter-level accuracy; however, the availability of these methods is much less than the desired value [1]. In addition, the use of PPP is faced with the issue of convergence time [2]. Currently, the use of PPP on the sea is expected because there are no obstacles and RTK-GNSS is impossible without base stations. The presence of buildings and trees induces signal reflections and attenuations, which affect the measurements. In extreme cases, the number of visible satellites is

insufficient, and the receivers are unable to provide the position velocity and time data, thus presenting a serious disadvantage to the GNSS. As a result, the advance driver-assistance system (ADAS) relies on light detection and ranging, and some devices such as camera, and radar. Therefore, determining the absolute position information, as well as the lane a vehicle is in, is important for proper functioning of these devices. For example, camera sometimes cannot recognize the lane since the white line has disappeared. To overcome the difficulties in determining the location in urban environments, some excellent studies have been conducted on both the GNSS, and GNSS with other sensors. Previous studies have proposed various innovative signal processing techniques to mitigate the multipath errors [3-5] and high-sensitivity receivers that can be used in closed environments [6]. To reduce the effect of non- line of sight (NLOS) signals, 3D building models [7] and fish-eye view camera information [8] can be used. Moreover, the integration of the GNSS with other sensors is essential because it is either impossible or difficult for the GNSS to provide reliable position information in areas such as overpass, tunnels, deep forest, and dense urban environments. Small, robust, and low-cost inertial sensors (e.g., micro electrical mechanical sensors (MEMS) [9]) have been available in the market for several years and are available together with GNSS receivers, especially for land vehicle navigation. In the last decade, different approaches for GPS/INS integration have been developed [10], many of which have been investigated for different grades of inertial measurement units (IMUs). The three most common integration strategies include the loosely coupled [11], tightly coupled [12], and ultra-tight integration [13] strategies. When we look at the GNSS/INS integration, there are many works related to DGNSS/INS or RTK-GNSS/INS integration. However, CLAS/INS integration is not evaluated because wide-area RTK service is not so practical in the world.

In this study, current performance of CLAS and PPP services through QZSS were evaluated on the sea. Since the correction data can be received from QZSS, all we need is just receiver capable of QZSS L6 signal decoding and CLAS/PPP solutions. Then, we evaluated the integration method of CLAS with IMU/Odometer. This is the main point in this study. A CLAS/IMU sensor and an odometer of a car are used in loosely coupled integration. The CLAS is mainly used for positioning because the convergence time is fast. If the speed information is obtained, the position information can be generated continuously as long as the attitude of the car is estimated correctly using IMU, although the position error increases with time without GNSS. Once the decimeter-level position of CLAS is obtained, maintaining approximately 1 to 2 m level position using IMU/Speed sensors for at least 1 min is not very difficult. In fact, the error of Doppler frequency easily exceeds 1 Hz, which indicates that a larger than 20 cm/s error in a single epoch might occur. Observing the correction of IMU from GNSS measurements, it is clearly difficult to correct biases of IMU in the case of poor signal conditions. It is known that the error of yaw angle should be kept within 0.1 to 0.2 degree in terms of 1 to 2 m level position for 1 minute. Unfortunately, 1 Hz error of Doppler frequency does not contribute to the bias correction of IMU. Therefore, the accuracy and stability of the IMU are very important for a continuous high accurate positioning.

This paper is organized as follows: The first section defines the aim of this paper in Introduction. Secondly, the outline of QZSS and correction services which means CLAS/PPP are introduced. Then, the integration method for filtered velocity estimation is discussed. After that, the integration of CLAS with the filtered velocity information is discussed. Then, the paper describes the first results of experiment using CLAS/PPP performed on the sea in Tokyo Bay. Also we describe the second results of experiment using CLAS performed in expressway in Tokyo. In the last section, we conclude our study. As for the test results of MADOCA with IMU/Odometer, please refer to the proceedings of Pacific ION 2019 [14].

QUASI-ZENITH SATELLITE SYSTEM (QZSS)

The QZSS is a Japanese regional navigation satellite system (RNSS) that has been operated as a four-satellite constellation since November 2018. Three QZSS satellites (QZS1, QZS2, QZS4) are in QZO (Quasi-Zenith Orbits) and one QZSS satellite (QZS3) is in a geostationary orbit (GEO) as shown in Figure 1. The QZSS is available in East Asia, Southeast Asia, and Oceania. Especially in East Asia, the QZSS can be observed at a high elevation angle for a long time due to the QZO that its satellites follow. This, in turn, enables stable positioning and improved positioning accuracy even in urban or mountainous areas, where there are no open-sky environment with buildings or trees. The QZSS signals for positioning, navigation, and timing service (PNT) are compatible with GPS signals (L1C/A, L1C, L2C, L5), which increases the number of satellites on a multi-GNSS receiver. On the other hand, the QZSS transmits some unique augmentation signals (L1S, L6D, L6E) to improve positioning accuracy and these three types of augmentation signal have unique advantages and disadvantages and usage.

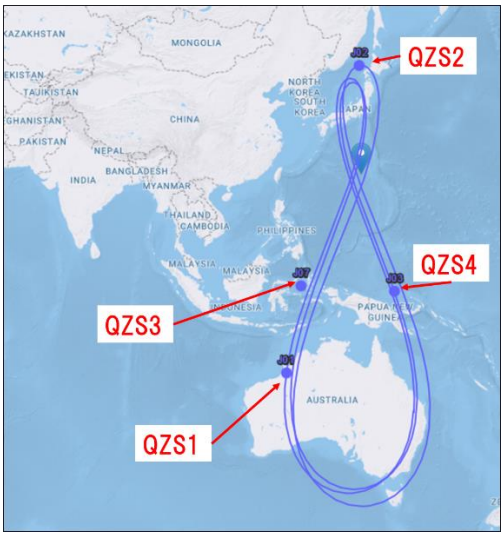

Figure 1. The orbit of the Quasi-Zenith Satellite System

Table 1. The Quasi-Zenith Satellite System signals

Frequency	1176.45MHz		1227.60MHz	1278.75MHz		1575.42MHz			
QZSS	L5	L5S	L2C	L6D	L6E	L1C/A	L1C	L1S	L1Sb
	PNT	Positioning Technology Verification Service	PNT	Centimeter-Level Augmentation Service (CLAS)	Multi-GNSS Advanced Demonstration tool for Orbit and Clock Analysis (MADOCA)	PNT	PNT	Sub-meter Level Augmentation Service (SLAS)	SBAS
GPS	L5		L2C			L1C/A	L1C		
	PNT		PNT			PNT	PNT		
Galileo	E5a			E6B	E6C	E1			
	PNT			High-Accuracy Service (HAS)	Commercial Authentication Service (CAS)	PNT			

The sub-meter level augmentation service (SLAS) that uses the L1S signal was developed to replace the existing coastal radio beacon DGPS service; L1S contains pseudo-range error information arising from the satellite's orbit and clock error, as well as ionospheric and tropospheric delay. It can reduce position error on a single-frequency receiver because its own frequency is the same as that of L1C/A. This service is expected to be used mainly in ships, cars, and smartphones that require sub-meter level accuracy at a low cost. However, we have not discussed the details of the SLAS system or evaluated it in this paper.

CLAS service

The centimeter-level augmentation service (CLAS) that uses the L6D signal was developed for highly precise positioning measurements, such as real-time kinematic positioning (RTK), that covers all of the Japanese territory. Figure 2 shows the coverage area of CLAS. The L6D signal broadcasts correction data on orbit, clock, ionosphere, troposphere, and code/carrier phase biases of GPS L1/L2, QZSS L1/L2, and Galileo E1/E5. These correction data are calculated from Japanese continuously operating reference station (CORS) network and compressed to the compact format of state space representation (SSR) to transmit over the limited bandwidth L6D signal from QZSS. When the CLAS receiver receives the L6D signal, its receiver decodes the L6D signal to compact SSR and then converts it to an observation state representation (OSR) form according to its approximate user position. Precise position is calculated by the PPP-RTK method using this OSR and a carrier-phase. A major feature of CLAS is that it broadcasts local ionospheric and tropospheric correction information which is different in each 60-km grid, which enables fast time to first fix (TTFF). The official performance standard of CLAS position error is shown in Table 2 [15]. This error value is the same as 2DRMS (twice the distance root mean square) and its value means 95% confidence interval of all positioning errors. The TTFF is the average time taken to solve the ambiguity in the carrier-phase and the output centimeter-level position after the L6D signal is received. Availability indicates the probability of a user in Japan to receive healthy L6D signal from at least three QZSS satellites.

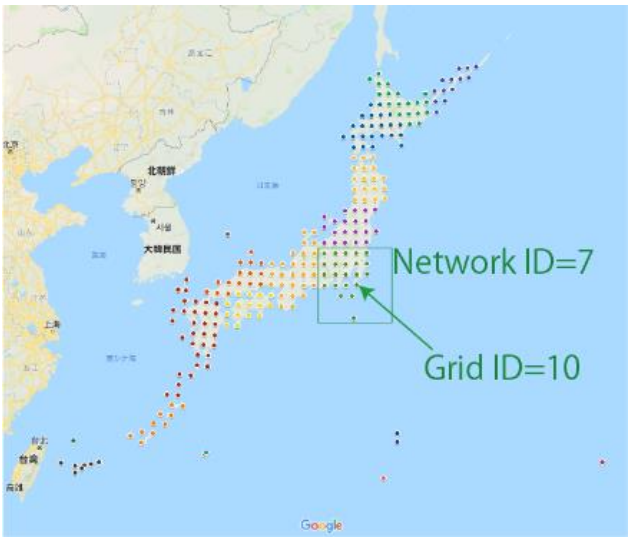

Figure 2. Coverage area of CLAS

Table 2. The CLAS performance standard

User Type	Position Error		TTFF	Availability
	Horizontal	Vertical		
Static	≤6cm (95%)	≤12cm (95%)	60 sec	≥0.99
Moving	≤12cm (95%)	≤24cm (95%)		

Suitable uses for the CLAS are in IT-construction (mapping and construction machine operation), agriculture (management and agricultural machine operation), and coastal maritime sectors, such as efficient ship birthing, coastal construction, and coastal survey. The CLAS has the potential to replace the VRS service or the precise positioning (PPP) service that receives the GNSS correction data via satellites or the internet, which is very expensive but used by users, who need precise position in the coastal area.

MADOCA-PPP service

The multi-GNSS advanced demonstration tool for orbit and clock analysis (MADOCA) uses the L6E signal; this system is being tested for high precision PPP, which is available wherever the QZSS can be observed. The overall configuration is shown in Figure 3. The L6E signal broadcasts correction data of orbit and clock of GPS L1/L2, QZSS L1/L2, GLONASS G1/G2. As compared with the CLAS, the MADOCA does not augment local ionospheric and tropospheric delay, and thus, its receiver needs to estimate these delays by itself using ionosphere-free combination using dual-frequency (L1+L2 or L1+L5). This method has another disadvantage that it requires a certain time period to converge to decimeter-level accuracy. The performance standard of MADOCA is not confirmed yet because it is still under testing. The correction data of the satellite's orbit and clock error are calculated from the observational data from the MGM-net reference station that covers the Asia-Pacific region. This correction information is converted to the SSR format and then uploaded to the QZSS. The key feature of MADOCA is its real-time free PPP service that covers a wide area, not only in the Japanese territory but outside of it as well. It is suitable to be used in the network infrastructure of an undeveloped area, such as offshore regions. For example, PPP buoy for early tsunami detection was demonstrated far offshore of Japan [16].

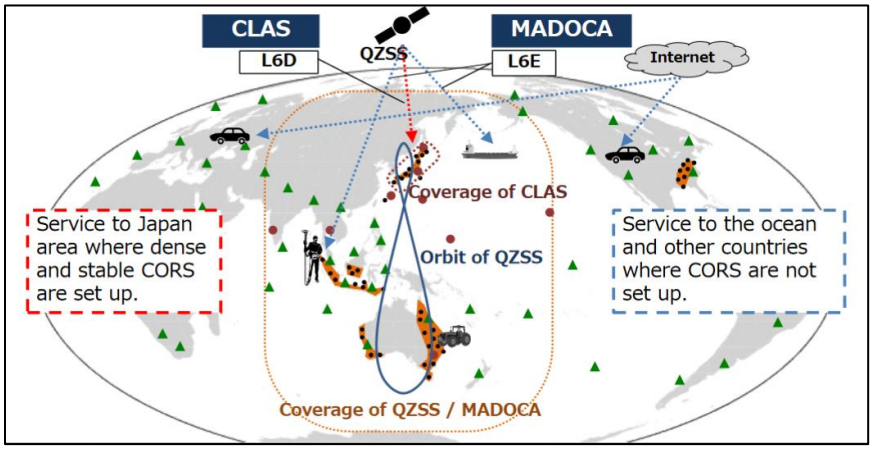

Figure 3. Coverage of MADOCA and its reference stations

FILTERD VELOCITY AND POSITION ESTIMATION

Loosely coupled velocity estimation algorithm is briefly introduced in this section. The block diagram of loosely coupled integration is shown in Figure 4. There are 4 inputs shown in gray blocks. The final output is filtered velocity and position. Angular velocity is obtained as the output of low-cost commercial IMUs, and zero velocity updates (ZUPTs) are applied for their measurements. A conventional method was used to remove the IMU bias. In case of zero velocity of the car, the change in angular velocity should be zero. If the ZUPTs are not applied to the IMU outputs, the IMU error increases significantly and affects the accuracy of integration. The temperature based correction of angular velocity is also applied in this test. The speed sensor equipped in the vehicle is used to obtain the distance information of the car. Normally, a velocity pulse generation equipment counts the number of pulses per rotation of the wheel. This number is usually 4 or 8, but it has been increased for the purpose of ADAS because it requires more accurate distance measurement. In this study, we use the speed pulse obtained from the POSLVX, which is a wheel-mounted rotary shaft encoder that accurately measures the linear distance covered by the vehicle [17]. The GNSS receiver provides the complete position and velocity information. Heading is estimated using velocity information when there is a movement, because it is impossible to estimate heading while the car is not in motion. The Kalman filter is used to integrate the heading or pitching information obtained from the gyroscope with the velocity. The velocity is estimated using both GNSS-derived velocity and scalar speed from the vehicle sensor. If the information from GNSS is not available due to enclosed environments such as tunnels, we only rely on the information from the IMU and speed sensor. The part of position estimation is introduced in the later section.

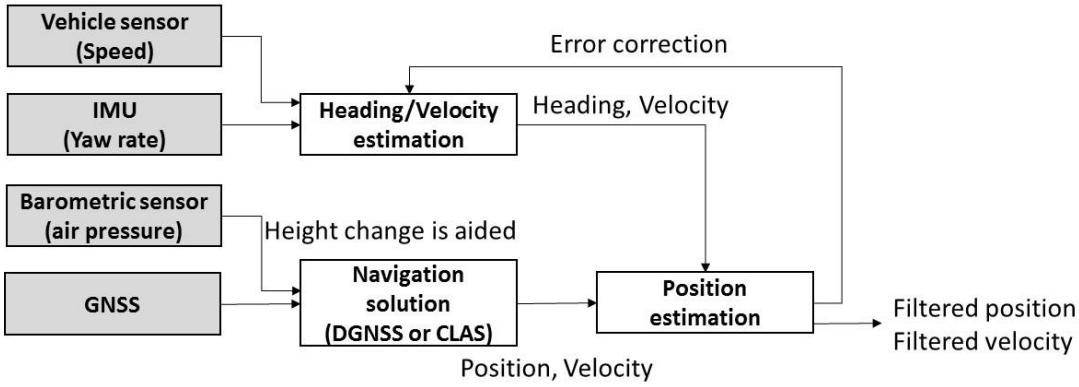

Figure 4. Block diagram of loosely coupled velocity integration

Heading estimation

A yaw rate gyroscope provides the measurement of the true turning rate together with the moving bias and zero mean, i.e., white noise. The true yaw rate and bias can be modeled as follows:

$$\begin{aligned} \dot{\Psi} &= r - b_g - \omega_g \\ \dot{b}_g &= \omega_b \end{aligned} \tag{1}$$

where, $\dot{\Psi}$ is the true yaw rate of the vehicle, r is the measured yaw rate, b_g is the yaw rate gyroscope bias, ω_g (ω_g ~N $(0, \sigma_g^2)$) is the yaw rate gyro noise, and ω_b (ω_b ~N $(0, \sigma_b^2)$) is the noise driving the bias drift. The measurement heading obtained from the GNSS comprises the true heading and zero mean white noise ($v = N(0, \sigma_\Psi^2)$), if the sideslip is assumed to be zero. The heading of the GNSS can be modeled as follows:

$$\psi_{GNSS} = \psi + v \tag{2}$$

The accuracy of the heading obtained only from the GNSS depends on the velocity measurements and partly on the dilution of precision (DOP). When the speed of the vehicle is low, the heading from GNSS alone is not reliable because the GNSS velocity measurement contains noise of a few centimeters per second. In addition, the sampling rate of GNSS is less than that of the yaw rate gyro; therefore, when the road curves suddenly, the obtained heading will contain an error. To obtain the accurate position during

GNSS outage, removing the heading bias of the IMU is very important. We propose several thresholds to be considered, to remove a heading bias if the moving state of the vehicle is as follows:

1) The vehicle speed is less than the speed threshold (4 m/s)
2) The horizontal dilution of precision (HDOP) is greater than the DOP threshold (2: HDOP)
3) The yaw rate is greater than the yaw rate threshold (4° /s)
4) The difference between the speeds obtained from the GNSS and vehicle sensor is greater than the threshold (0.25 m/s)

In the case of above these 4 conditions, GNSS is not used. Figure 4 shows the error of heading when the velocity is obtained from the low-cost GNSS receiver in dense urban areas. The reference heading is obtained from the POSLVX. Although several thresholds are set to remove large noise and error from the GNSS, as mentioned above, large heading errors can still be observed. This can be attributed to two reasons: the accuracy of the Doppler frequency of the low-cost GNSS receiver, and the heavy multipath errors under many high-rise buildings. In fact, the DGNSS errors easily exceed 100 m. The usable number of headings from GNSS is about 28.5% in total. The maximum period that the GNSS-derived heading was unable to be used continuously was 143 s. This indicates that the IMU-based heading cannot be corrected for at least 143 s. If only the GPS satellites are used, the usable number of headings obtained from the GPS is 0%. The use of multi-GNSS is clearly vital. The yaw rate gyro of the IMU is used to calculate the heading during a GNSS outage. A prolonged outage will lead to an increase in the heading error if only the yaw rate gyro is used. To achieve the best heading accuracy of, we use a Kalman filter to integrate the GNSS-based heading with the IMU-based heading. The heading from the GNSS will also be used and the measurement covariance will be updated in each state.
The state vector to integrate the GNSS-based heading with the IMU-based heading can be constructed as follows:

$$x = \left(\psi_{GNSS}, \omega_{yaw}\right)^T \tag{3}$$

where, ω_{yaw} is the yaw rate obtained from the IMU. The state equation and measurement equation for a Kalman filter are as follows:

$$\begin{gathered} x_k = F_k x_{k-1} + G_k w_k \\ y_k = H_k x_k + v_k \\ F = \begin{bmatrix} 1 & \Delta t \\ 0 & 1 \end{bmatrix} \end{gathered} \tag{4}$$

where, F is the state transition matric and Δt is the interval of time. The accuracy metric for the GNSS-based heading is defined below:

$$\sigma_{\psi_{GNSS}} = \frac{\sigma_{v_{GNSS}}}{speed} \tag{5}$$

where, $\sigma_{v_{GNSS}}$ is the GNSS speed accuracy and speed denotes the speed of the vehicle. The covariance matrix is as follows:

$$R = \begin{bmatrix} \sigma^2_{\psi_{GNSS}} & 0 \\ 0 & \sigma^2_{\omega_{yaw}} \end{bmatrix} = \begin{bmatrix} \sigma^2_{v_{GNSS}}/speed & 0 \\ 0 & \sigma^2_{\omega_{yaw}} \end{bmatrix} \tag{6}$$

The heading measurement is bounded from 0 to 2π . The error must be corrected between the two measurements obtained from the GNSS and IMU. As the first step, the ZUPT is applied to the IMU outputs. The last accurate heading estimation obtained from the GNSS, after checking the above four thresholds, is fed into the Kalman filter as the measurement data. An important quality check of the heading obtained from the GNSS must be performed as follows: as seen from the GNSS heading estimation in Figure 5, large errors of the heading obtained from the GNSS should not be used in the integration. Therefore, the heading from the GNSS must always be checked using both the best estimated heading in the previous epoch and yaw rate, because the yaw rate obtained from the IMU in a short period is very accurate and stable. The threshold in the proposed method is 2°. The final integrated heading errors are shown in Figure 6. The standard deviation of these errors is 0.26° and the total bias is 0.011°. The IMU sensor used in this paper is GSM-MG100 manufactured by the Tokyo Aircraft Instrument Cooperation, which is a relatively high-grade low-cost Micro-Electro-

Mechanical System (MEMS) sensor. The raw 3-axis angular rate, 3-axis acceleration, and pressure are provided. Angular rate and pressure outputs are used in this paper. On evaluating the summation of the yaw rate angle for 1 h with the first 1-min bias removal, the typical stability performance of the yaw angle is found to be approximately 5° to 10°.

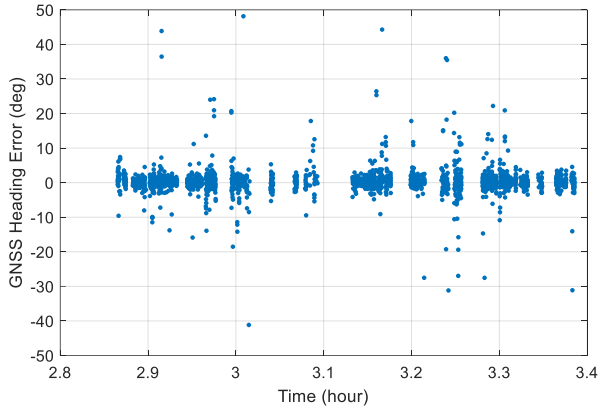

Figure 5. Heading error obtained from the GNSS

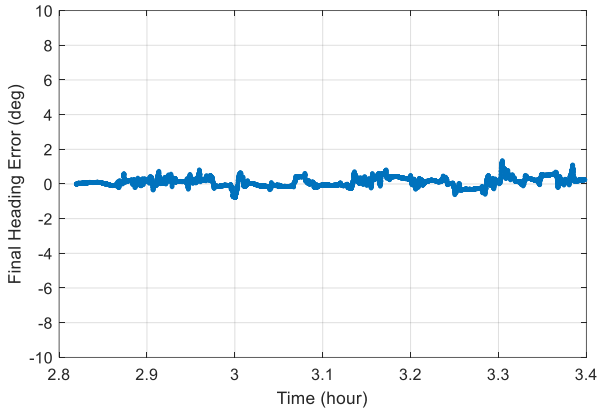

Figure 6. Final integrated heading errors

Since the filtered heading is already estimated in the above, it is easy to generate the 2D velocity vector from IMU and speed sensors. With heading and speed information, 2D velocity vector can be estimated. On the other hand, 2D velocity vector from GNSS Doppler frequency is also available as long as we move in the relatively open sky condition. The accuracy of the velocity information of GNSS is approximately cm/s level. However, when we move in the vicinity of the obstacle such as overpass and high-rise building, the accuracy deteriorates easily. Therefore, it is important to integrate those two velocities deduced from different sources using Kalman filter. Furthermore, if the velocity vector of GNSS is not reliable, we rely on the velocity vector from both heading and speed sensors. In addition to the horizontal velocity, the vertical velocity is also integrated in the similar way. At that time, pitch angle from IMU and vertical velocity from GNSS are integrated using Kalman filter. The IMU sensor used in this paper includes a barometric sensor and it is also used in the vertical velocity estimation.

Position estimation

An outline of the position estimation is described here. First, the coordinate frame rotation and translation are considered. Three frames were considered, namely the earth-centered earth-fixed (ECEF) coordinate frame, body frame, and the north east down (NED) coordinate frame. The origin of the ECEF frame is the center of mass of the earth; the x-axis is toward the 0° latitude (equator) and 0° longitude (Greenwich), the y-axis is toward the 0° latitude (equator) and 90° longitude, and the z-axis is parallel to the earth's mean spin axis. The origin of the body frame is the center of the vehicle; the x-axis is toward the north, the y-axis is toward the east, and the z-axis is parallel to the gravity of the vehicle. Rotation matrices are required to rotate the coordinates between two sets.

Figure 7 presents a simple basic system and estimation parameters for Kalman filtering. Figure 8 shows a portion of Kalman filtering that includes prediction, correction, and Kalman gain. Three-dimensional positions can be estimated using these equations. The inputs of this system are based on the NED coordinate system, which means that x is the longitudinal direction, y is the latitudinal direction, and z is the vertical direction. The 3D position of the GNSS base station is set to the origin (0, 0, 0). The velocity vector is also based on the same coordinate system. More importantly, if a low-cost barometric sensor is used, the vertical position of the GNSS is integrated with the change in the vertical position deduced from the barometric sensor. With a low-cost barometric sensor, even in dense urban areas, an accuracy of about 1 to 3 m of the altitude can be easily achieved. The IMU sensor used in this paper includes a barometric sensor and it is also used in the height estimation. If the velocity vector estimated by the GNSS is not available or is contaminated by noise and errors, the velocity vector estimated by the final integrated heading and speed sensor is used instead. If the absolute difference between these two velocity vectors is more than about 0.25 m/s, we rely on the velocity vector estimated by the final integrated heading and speed sensor. Regarding the standard deviation as an input to the Kalman filter, the absolute positions from the DGNSS and CLAS are set as 1 m and 1 cm, respectively, and the velocity information is set as 2.5 cm/s.

Besides this algorithm, a simple dead reckoning using the previously estimated position by Kalman filtering and velocity vector is newly implemented in addition. To realize the proposed method, the output (x', y', z') of dead reckoning calculated in addition is used. When the absolute difference between the dead reckoning positions and the code-based DGNSS positions is more than 3 m and 5 m for semi-urban areas and dense urban areas, respectively, we do not rely on the positions as the input because the pseudo-range observations are highly deteriorated by a strong multipath. We simply adjust the weighting between (x, y, z) and (x', y', z') according to the absolute difference. When the positions (x, y, z) are not relied upon, the standard deviation of the Kalman filter is varied for the absolute position according to the magnitude of the estimated difference. Because the CLAS position is available, we use this method to remove the wrongly fixed positions with large errors. The threshold must be set according to the environment and IMU accuracy. An outline of this new method is shown in Figure 9. This method is very effective in reducing the outliers from GNSS-based positions obtained from the DGNSS as well as CLAS. The limitation of this method depends on the IMU accuracy. From several tests, it was observed that approximately continuous 1-min dead reckoning is sufficient and acceptable in terms of 1 to 2 m position accuracy. With a prolonged outage of the GNSS of more than 1−2 min due to enclosed areas such as long tunnels, it is very important to reset the Kalman filtering appropriately.

$$\boldsymbol{x}_{k+1} = \boldsymbol{F}\boldsymbol{x}_k + \boldsymbol{G}\boldsymbol{w}_k$$

$$\boldsymbol{y}_k = \boldsymbol{H}\boldsymbol{x}_k + \boldsymbol{v}_k$$

$$\boldsymbol{x_k} = [x(k), y(k), z(k), v_x(k), v_y(k), v_z(k)]^T$$

$$x(k+1) = x(k) + v_x(k)\Delta t$$

$$y(k+1) = y(k) + v_y(k)\Delta t$$

$$z(k+1) = z(k) + v_z(k)\Delta t$$

$$\boldsymbol{F} = \begin{bmatrix} 1 & 0 & 0 & \Delta t & 0 & 0 \\ 0 & 1 & 0 & 0 & \Delta t & 0 \\ 0 & 0 & 1 & 0 & 0 & \Delta t \end{bmatrix}$$

$$\boldsymbol{H} = \begin{bmatrix} 1 & 0 & 0 \\ 0 & 1 & 0 \\ 0 & 0 & 1 \end{bmatrix}$$

x_k: state vector

w_k: system noise

y_k: measurement vector

v_k: measurement noise

F: state transition matrix

G: noise distribution matrix

H: observation matrix

Figure 7. Basic system and estimation parameters

$$\hat{\boldsymbol{x}}_{k|k} = \hat{\boldsymbol{x}}_{k|k-1} + \boldsymbol{K}_k(\boldsymbol{y}_k - \boldsymbol{H}_k\hat{\boldsymbol{x}}_{k|k-1})$$

$$\boldsymbol{P}_{k|k} = \boldsymbol{P}_{k|k-1} - \boldsymbol{K}_k\boldsymbol{H}_k\boldsymbol{P}_{k|k-1}$$

$$\boldsymbol{K}_k = \boldsymbol{P}_{k|k-1}\boldsymbol{H}_k^T(\boldsymbol{I} + \boldsymbol{H}_k\boldsymbol{P}_{k|k-1}\boldsymbol{H}_k^T)^{-1}$$

$$\hat{\boldsymbol{x}}_{k+1|k} = \boldsymbol{F}_k\hat{\boldsymbol{x}}_{k|k}$$

$$\boldsymbol{P}_{k+1|k} = \boldsymbol{F}_k\boldsymbol{P}_{k|k}\boldsymbol{F}_k^T + \sigma_w^2/\sigma_v^2\Lambda$$

$$\Lambda = GG^T = diag\{0,0,0,1,1,1\}$$

Figure 8. Kalman filtering

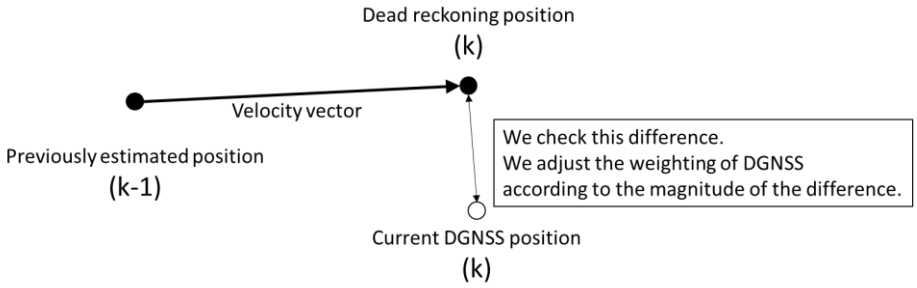

Figure 9. Newly implemented outlier detection

TEST ON THE SEA

Test area and voyage

The test was conducted using a training ship, Shioji-maru, that belonged to Tokyo University of Marine Science and Technology. The gross tonnage of this ship is 425 t, and its length is almost 50 m. Figure 10 shows the picture of We tested the two services under question with this ship during two voyages in the Tokyo bay area shown in Figure 11 and Figure 12. Maximum speed over ground (SOG) was almost 8 kn during voyage 1 and 10 kn during voyage 2

Figure 10. Shioji-maru

Figure 11. Test voyage

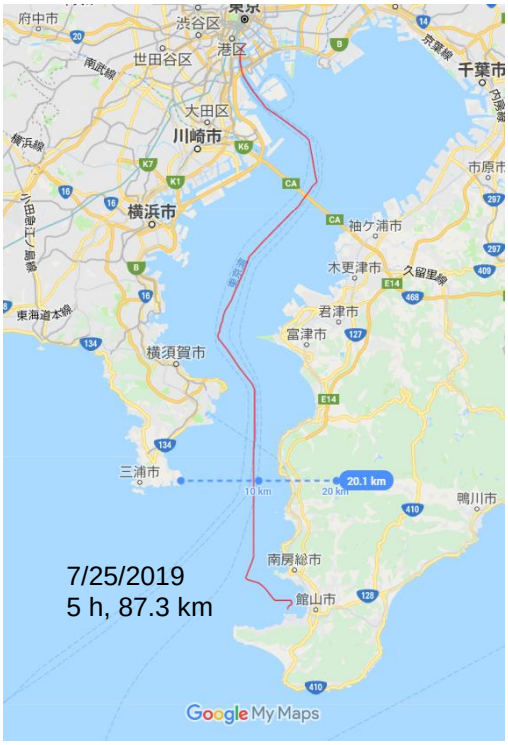

Figure 12. Test voyage

Configuration of the GNSS receiver

We evaluated CLAS and MADOCA in the configurations shown in Figure 13. The MSJ receiver is a commercial L6-supported receiver, i.e., MJ-3021-GM4-QZS-EVK, that was developed by Magellan Systems Japan. We used two receivers: one for CLAS and another one for MADOCA. The GNSS antenna on the ship is an accessory multi-band antenna of the MSJ receiver. Trimble SPS855 RTK receiver was used to get the RTK position using correction data from the base station at Tokyo University of Marine Science and Technology. The RTK position by this Trimble high-end receiver was at a 1-cm-level accuracy. We used this as a reference true

antenna position on the ship. The GNSS antenna was installed on the compass deck of the ship shown in Figure 14. This position was similar to the GNSS/GPS antenna used on commercial vessels, and this position has a probability that some GNSS signal will be blocked by radar mast and multipath occurrence. Three receivers were installed in the bridge room and were connected to the same GNSS antenna through a signal splitter.

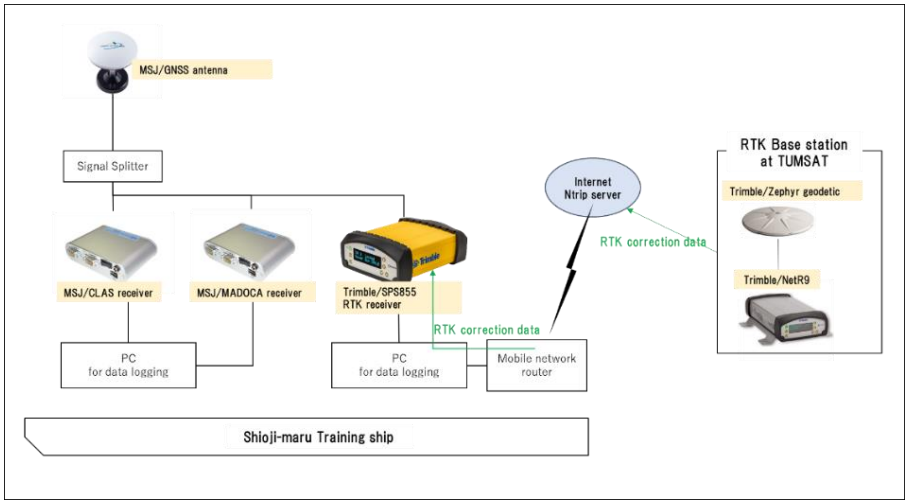

Figure 13. Configuration of the GNSS

Figure 14. GNSS antenna

RESULTS ON THE SEA

The reference position for evaluation of MADOCA and CLAS

First, we confirmed the RTK result accuracy by using SPS855 because the southernmost point of the voyage was 75 km far from the RTK base station. To confirm the accuracy of the RTK, we calculated post-process RTK with nearest CORS data to compare these results. The Fix rate (percentage of cm-level position solutions) of RTK with the TUMAST base station was 98%. The standard deviation of the difference between the two results was 1.3 cm along the longitude, 1.1 cm along the latitude, and 2.8 cm along the vertical axis. Thus, we confirmed that the RTK result of SPS855 was not degraded so much because of the long baseline distance from the base station, but it was enough to estimate the true ship position as an evaluation reference.

Evaluation of CLAS

The CLAS position error is shown in Figure 15 and Figure 16. The green plot indicates PPP-RTK Fix (cm-level position solutions), the yellow plot indicates PPP-RTK Float (cm-level position was not calculated), and the red plot indicates the single point positioning (SPP; augmentation was not applied). The 2DRMSE in Table 3 indicates that 95% error was under the 2DRMSE value and depicts the accuracy when PPP-RTK was Fix (only green plot). The official performance standard was 12 cm horizontally and 24 cm vertically, therefore, the test results were almost satisfied, except for the vertical result at voyage 2. The Fix rate during voyage 1 was lower than that during voyage 2. This was the relationship with quick ship maneuver. When the ship rotation rate was high, the positioning mode was changed to Float or SPP. In this test, the GNSS antenna was installed beside the radar mast; when the ship maneuver was quick, the mast could obstruct the GNSS signal tracking. However, it may be considered that this Float solution was not due to the L6 signal tracking loss, because even when the CLAS solution was Float, the L6 signal could be received with good signal strength.

Table 3. Fix rate and 2D RMSE

CLAS	Fix rate	Horizontal 2D RMSE	Vertical 2D RMSE
7/24 Voyage1	62.8 %	9.06 cm	25.76 cm
7/25 Voyage2	93.6 %	13.26 cm	34.78 cm

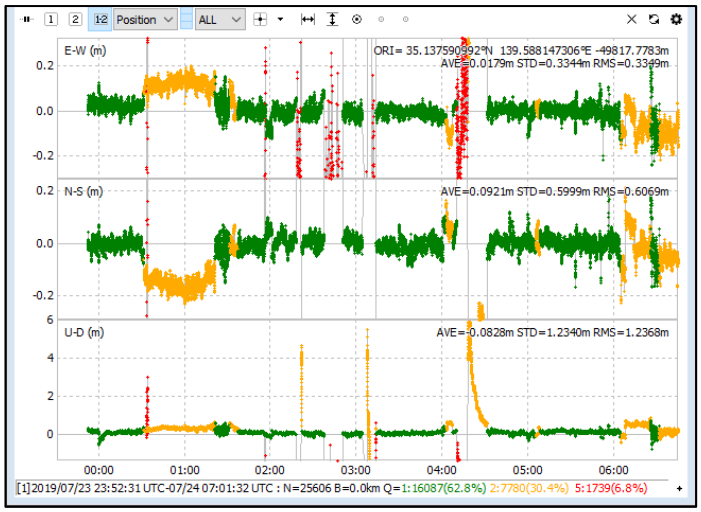

Figure 15. CLAS position error at voyage 1

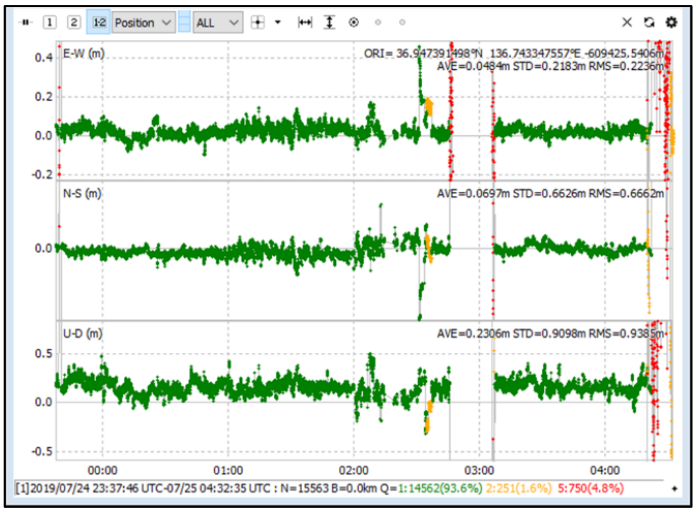

Figure 16. CLAS position error at voyage 2

Evaluation of MADOCA

The MADOCA position error is shown in Figure 17 and Figure 18. The yellow plot indicates the PPP and the red plot indicates the SPP. The PPP rate during voyage and 2DRMSE are shown in Table 4. During almost all epochs of the voyage the PPP by MADOCA could be calculated. However RMSE was worse than that of CLAS. It should be noted that these RMSE values included the error before convergence, when the atmospheric delay initialization by loss of tracking L6E signal or other reasons. From this result, we deduced that MADOCA-PPP should only be used after an atmospheric delay has been solved and to identify the convergent solution and non-convergent solution. We used the estimated error data output from the receiver to identify this. The estimated error synchronizes with the real error value and it is enable to remove large error solution by monitoring it. Convergence time of MADOCA-PPP on the MSJ receiver is almost 10-12 minutes. Table 5 shows the PPP rate and 2DRMSE after removal of large error using the estimated error threshold of 20 cm. This shows MADOCA-PPP have lower than 50-cm-level accuracy on a ship by monitoring the estimated error.

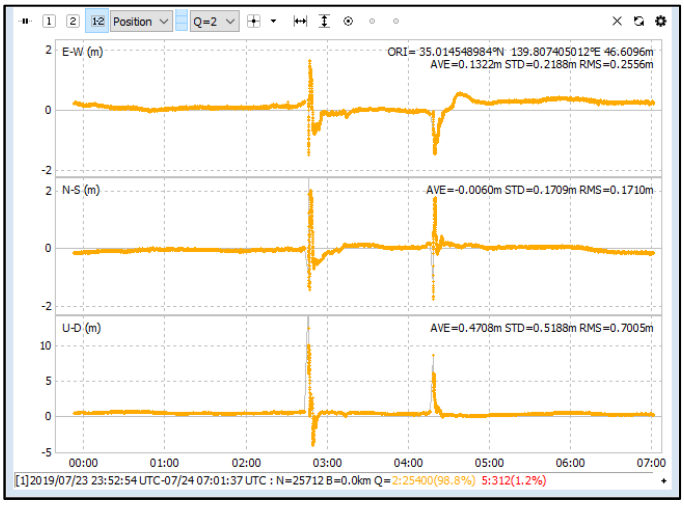

Figure 17. MADOCA position error at voyage 1

Figure 18. MADOCA position error at voyage 2

Table 4. The PPP rate and 2DRMSE

MADOCA	PPP rate	Horizontal 2D RMSE	Vertical 2D RMSE
7/24 Voyage1	98.8 %	58.07 cm	127.44 cm
7/25 Voyage2	99.8 %	62.92 cm	116.46 cm

Table 5. The PPP rate and 2DRMSE (Only convergent solution)

MADOCA	PPP rate	Horizontal 2D RMSE	Vertical 2D RMSE
7/24 Voyage1	92.6 %	40.14 cm	31.34 cm
7/25 Voyage2	85.4 %	38.13 cm	28.78 cm

Test summary on the sea

We have evaluated the CLAS and MADOCA, high precise augmentation services by QZSS that use the L6 signal on a ship. The accuracy of CLAS was evaluated to be better than that of MADOCA, but its availability was different. There is no accuracy and availability degradation in the coastal area 5~10km away. Mast or other object on the ship blocked L6 signal and it caused somehow low fix rate. We should consider antenna install position or more robust L6 tracking selection algorithm. This is one of the problems associated with this system and a future task of the CLAS receiver because the RTK by Trimble SPS855 produces a 100% Fix solution using the same antenna although the number of used satellites was different. The MADOCA-PPP could constantly provide a 40-cm-level solution, except for a few times, when a large error was seen because of atmospheric delay estimation initialization and vertical position bias. This large error was removed by monitoring estimated error that was calculated by the receiver and modification to remove vertical bias. We expect that sufficient accuracy was achieved in the whole coverage area of QZSS and that it can become a strong precise positioning tool in the oceans of the Asia-Pacific region. Future tasks regarding MADOCA are to conduct more evaluations in different regions, especially tropical areas, where the atmospheric influence on GNSS is strong, and to perform modification on its receiver to achieve faster solution convergence.

TEST ON THE EXPRESSWAY

This section describes the expressway scenario of the experiments and discusses the results in detail. The scenario includes normal urban areas and relatively open sky area in metropolitan expressway. There are some overpasses. The raw data of GNSS, IMU, and speed sensors are post-processed using our algorithm mentioned above. This processing is quick and can be used in real time. For the correction data, internet based correction of CLAS was used. The GNSS receiver capable of CLAS positioning used in this test was Chronosphere-L6S manufactured by CORE Corporation. This receiver was used to produce real-time CLAS positioning. For the normal code based DGNSS and velocity output, F9P receiver manufactured by u-blox was used simultaneously.

The experiment was performed in an expressway environment near our campus in Tokyo, Japan, in September 2018. The configuration of the sensors used in this test is provided in Table 6. The model of the car used was SUBARU IMPREZA 2019, and the sampling rate of the position data was 5 Hz. The sampling rate of IMU and speed sensors was 100 Hz. The satellite system and frequency used in this test were GPS/QZSS L1C/A and L2P or L2C, Galileo E1 and E5a for CLAS. GPS/QZSS L1C/A, Galileo E1, GLONASS G1 and BDS B1 were used for DGNSS and velocity estimation. The IMU sensor provides the 3-axis angular rate, 3-axis acceleration, and pressure with GPSTIME. The total data recording period was 3,150 s. The POSLVX (Applanix) was used to estimate the reference position and heading to recognize the temporal errors deduced from our proposed method. The two receivers shown in Table 6 were connected to the same antenna. The IMU was set up in the center console box in the car. The test course is shown in Figure 19. The first 10 minutes was normal urban areas shown in red circle. After that, we got on the expressway. 2 lanes were present on each side of the road and several short overpasses were present in the test environment. In addition, two long overpasses were also present. To evaluate the performance of the filtered velocity vector shown in the block diagram of Figure 4, the position was generated by only accumulating the velocity vector; the temporal errors are shown in Figure 20. The horizontal accuracy was maintained at less than 30 m.

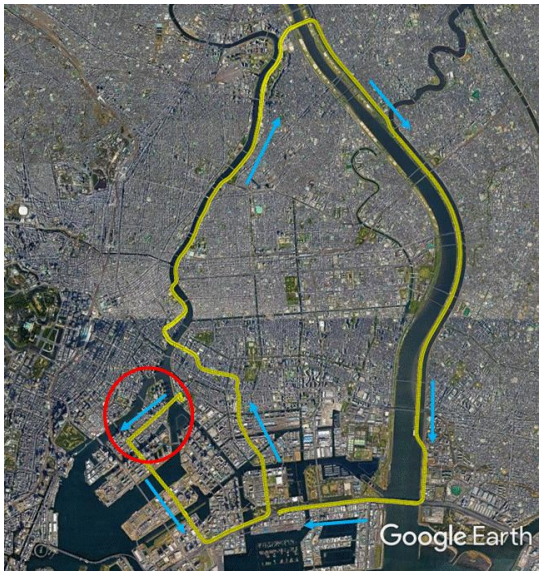

Figure 19. Test course in the expressway

Table 6. Configuration of the sensors used in test

Sensor	Model name
GNSS receiver (CLAS)	Core Chronosphere-L6S
GNSS receiver (DGNSS and velocity output)	u-blox F9P
GNSS antenna	JAVAD GrAnt-G5T
GNSS antenna (base)	Trimble Zephyr 2 Geodetic
IMU (MEMS)	TKK CSM-MG100
Speed	Equipped in wheel (over 100 PPR)
Reference position	Applanix POSLVX
Base station	Trimble NetR9

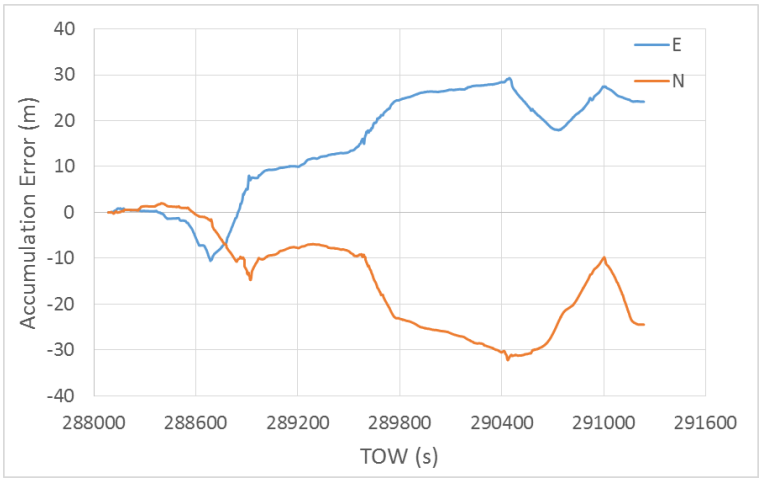

Figure 20. Accumulated position errors of filtered velocity vector

Figure 21 shows the coordinate errors of fixed positions of CLAS deduced by Core Chronosphere-L6S. The fixed rate was 72.0 % and there were no large wrong fixed errors over 20 cm although there were several overpasses and buildings. Figure 22 shows the coordinate errors of DGNSS positions deduced by observation data of u-blox F9P. The DGNSS positioning rate was 98.4 %. As can be seen from this figure 22, there are large errors for the first 10 minutes while we drove in urban areas and two times large errors clearly happened in the two long GNSS outage periods under overpasses. The maximum horizontal errors reached about 60 m and horizontal errors during relatively open sky condition on the expressway was mostly below 1 m. DGNSS positioning itself was post-processed by our program same as the velocity estimation. The mask angle was 15 degrees and the minimum carrier to noise ratio was 35.0 dB-Hz. Figure 23 shows the final integrated navigation performance in terms of horizontal errors. As can be seen from this Figure 23, the maximum error was 2.1 m while we drove at the second long overpass and all solutions except for this overpass was less than 1.5 m. The standard deviation for the absolute horizontal errors was 0.35 m. Figure 24 shows the accumulated percent for the integrated navigation in terms of the absolute horizontal errors. The 99 percentile value for the absolute horizontal errors was 1.34 m. 99.6 % of all solutions were less than 1.5 m in horizontal.

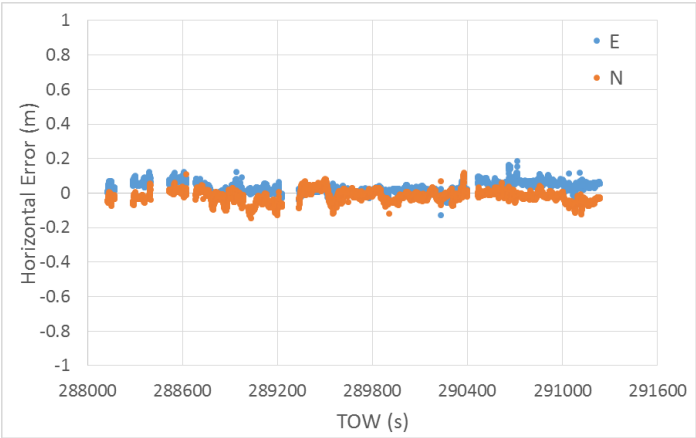

Figure 21. Horizontal errors of fixed positions of CLAS

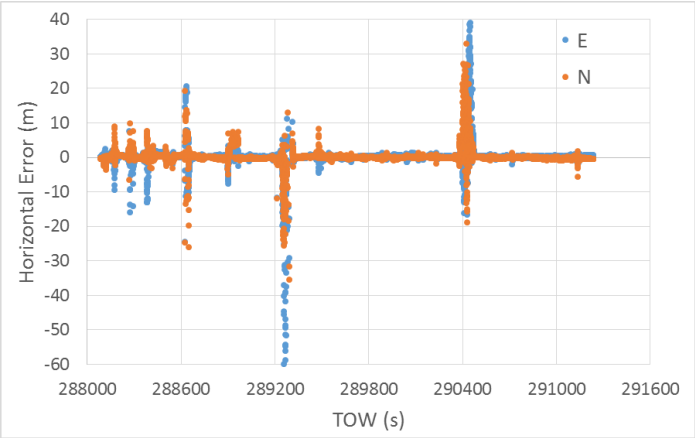

Figure 22. Horizontal errors of DGNSS

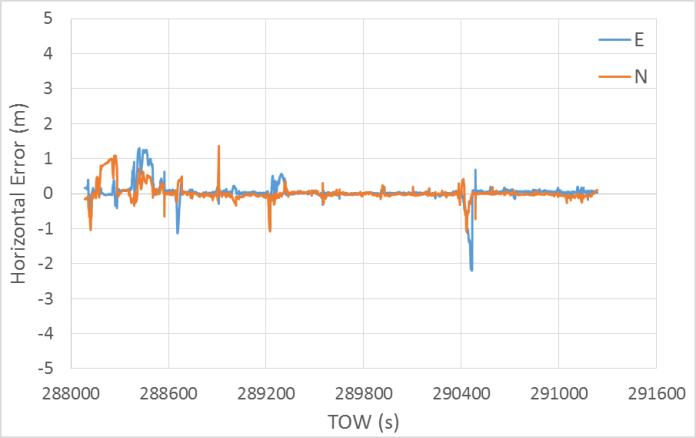

Figure 23. Horizontal errors of integrated navigation

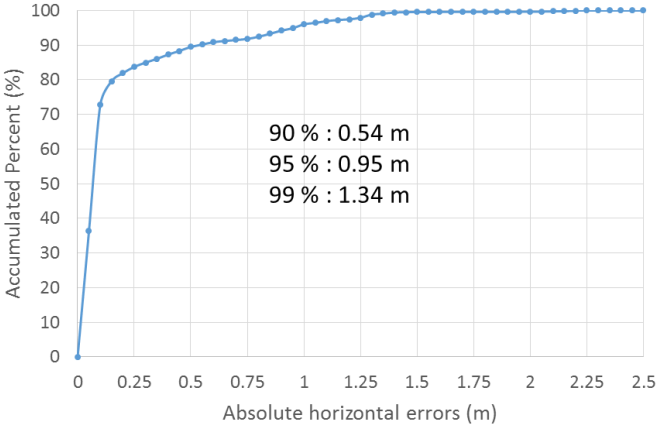

Figure 24. Accumulated percent of integrated navigation

Test summary on the expressway

We have evaluated the integrated navigation of CLAS and IMU/Odometer by using the car. The test course was mostly expressway in Tokyo including general road in urban areas. The CLAS performance itself was good and there were no large wrong fixes. The fix rate was 72.0 % and all horizontal errors were within 20 cm. The final integrated navigation was introduced and 99.6 % of all solutions were less than 1.5 m in horizontal. The integration navigation could constantly provide 20-cm-level solution in the case of relatively open sky condition. On the other hand, we have to cope with the long overpasses because the accuracy strongly depends on the grade of IMU sensors. When we look at the performance of CLAS, it was similar to the normal RTK performance in terms of using same GNSS and same frequency. In the near future, the maximum number of usable GNSS will increase from 11 to 17. Therefore, the performance of CLAS will be improved more and more.

CONCLUSION

We have investigated the performance of pure MADOCA-PPP, CLAS and the integration of CLAS with IMU/Odometer sensors. Firstly, only PPP and CLAS performance on the sea were introduced. MADOCA-PPP provides the continuous positions on the sea, however the accuracy of PPP was occasionally degraded due to the bridge. The convergence time is also the future task to improve. CLAS does not provide the continuous positions in terms of the fixed solutions. The accuracy of the fixed position was within 10 cm and it will be enough for the application on the sea. Improving the fix rate will be the future task. With regard to the integration of CLAS with IMU/Odometer sensors in the expressway, the overall performance was relatively good except for the ling overpasses.

Firstly, the filtered velocity was generated by integrating GNSS velocity with IMU/Odometer sensors and 3D velocity vector was given to aid CLAS solution. Then loosely coupled integration of CLAS with filtered velocity was introduced. The experiment was conducted in the expressway in Tokyo using the CLAS receiver, low-cost dual frequency receiver and low-cost IMU. Speed information was also obtained from the car. The navigation performance of this integrated system was analyzed and the horizontal accuracy in the relatively open sky condition including some GNSS outages was stable and within several 10 cm. The standard deviation for the absolute horizontal errors of all epochs was 0.35 m. The 99 percentile value for the absolute horizontal errors was 1.34 m. 99.6 % of all solutions were less than 1.5 m in horizontal.

Acknowledgements
This work was conducted by New Media Development Association supported by Japan Keirin Autorace foundation (JKA) and its promotion funds from KEIRIN RACE.

REFERENCES

1. Kubo, N.; Suzuki, T. "Performance Improvement of RTK-GNSS with IMU and Vehicle Speed Sensors", *IEICE* **2016**, E-99A, No. 1, 217-224
2. Laurichesse, D.; Blot, A. "Fast PPP Convergence Using Multi-Constellation and Triple-Frequency Ambiguity Resolution", *Proceedings of ION GNSS+* 2016, Portland, Oregon, USA, 12-16 September 2016, 2082-2088.
3. Van Dierendonck, A.J.; Fenton, P.; Ford, T. "Theory and Performance of Narrow Correlator Spacing in a GPS Receiver", Navigation. *Journal of the Institute of Navigation* Fall **1993**, Vol.39, No.3, 265-283.
4. Garin, L.; Van Diggelen F.; Rousseau J.M. "Strobe & Edge Correlator - Multipath Mitigation for Code", Proceedings of ION GPS 1996, Kansas City, MO, USA, 17-20 September 1996, 657-664.
5. Townsend B.; Van Nee D.J.; Fenton P.; Van Dierenconck K. "Performance Evaluation of the Multipath Estimating Delay Lock Loop", *Journal of the Institute of Navigation* Fall **1995**, Vol.42, No.3, 503-514.
6. Spangenberg, M.; Julien, O.; Calmettes, V.; Duchâteau, G. "Urban navigation system for automotive applications using HSGPS, inertial and wheel speed sensors", Proceedings of European Navigation conference GNSS 08, Toulouse, France, 23–25 April 2008.
7. Groves, P. "Solving the Urban Positioning Problem using 3D-Mapping-Aided GNSS", Proceedings of ION GNSS+ 2016, Portland, OR, USA, 12–16 September 2016, 1967-1984.
8. Suzuki, T; Kubo, N. "N-LOS GNSS Signal Detection Using Fish-Eye Camera for Vehicle Navigation in Urban Environments", Proceedings of ION GNSS+ 2014, Tampa, FL, USA, 8-12 September 2014, 1897-1906.
9. Aggarwal, P.; Syed, Z.; El-Sheimy, N. "MEMS-Based Integrated Navigation", Artech House Publisher: Norwood, UK, 2010.
10. Wagner, J.F.;Wieneke, T. "Integrating satellite and inertial navigation-conventional and new fusion approaches", *Control Eng. Pract.* **2003**, 11, 543–550.
11. Solimeno, A. "Low-Cost INS/GPS Data Fusion with Extended Kalman Filter for Airborne Applications", Master's Thesis, Universidad Tecnica de Lisboa, Lisbon, Portugal, July 2007.
12. Petovello, M. "Real-time Integration of a Tactical-Grade IMU and GPS for High-Accuracy Positioning and Navigation", Ph.D. Thesis, University of Calgary, Calgary, AL, Canada, April 2003.
13. Soloviev, A.; Van Graas, F.; Gunawardena, S. "Implementation of Deeply Integrated GPS/Low-Cost IMU for Acquisition and Tracking of Low CNR GPS Signals", Proceedings of ION-NTM, San Diego, CA, USA, 26–28 January 2004, 923–935.
14. Kubo, N.; Zhang, Y.;, Hatta, D. "", ION Pacific PNT, Honolulu, Hawaii, USA, 8-11 April 2019, 388-401
15. Cabinet Office (2018) : "Quasi-Zenith Satellite System Interface Specification Centimeter Level Augmentation Service (IS-QZSS-L6-001)"
16. Hiroaki Yamada, Yasuhiro Matsushita, Ryota Ioka, et al. (2015) : "DEVELOPMENT OF NEW GPS OCEAN WAVE METER AND DEMONSTRATION EXPERIMENTS FOR HYDROGRAPHIC PHENOMENON IN THE OFFSHORE", Journal of JSCE vol.71
17. Applanix POSLV. https://www.applanix.com/products/poslv.htm (accesses on 8 Dec. 2018)